Modeling Study of Image Formation with Point Sources

B.S.Bollepalli, M. Khan & F. Cerrina
Department of Electrical Engineering,
University of Wisconsin Madison,
Madison,WI-53435

Abstract

It is well known that a point source produces a small magnification of the mask pattern on the wafer due to divergence; the effect becomes especially noticeable at the corners and edges of the field. In this article we model the image formation due to a point source and compare the deviations of the aerial images and developed patterns, from those at the center of the field. We illustrate the behavior with several computational results.

1 Introduction

X-ray lithography offers a viable solution for the fabrication of nanostructures beyond 0.13μm. The conventional source for the generation of X-rays has been the synchrotron radiation with a wavelength centered around 1nm. There also has been research going on in the development of plasma sources in order to provide a more compact and frugal system for the fabrication of nanostructures using X-ray lithography [1,2,3,4]. In addition to these advantages, there are some inherent problems associated with a point source - namely power and large local and global divergences[5]. These are illustrated in Figure 1. It can be easily seen that the illumination for a pattern located at the edges and corners of the mask field is oblique. This can cause a shift in the location of the developed feature on the resist and possibly distort the pattern. These are the prime aspects of our study in this paper.

The rest of the paper is organized as follows. First, we describe the modeling of the point source followed by the modeling of image formation. Then we consider typical divergence angles from point sources and compute the aerial images and developed patterns.

2 Some Modeling Aspects

The propagation of incident radiation through the mask, gap and onto the resist is modeled using a plane wave propagation method. The incident radiation on the mask, from a point source can consist of several isolated wavelengths. Figure 2 shows such a spectrum. For a mask pattern at a corner or edge of mask field, each of the wavelengths are incident at an

angle called the global divergence angle θ_g. Some common values of θ_g are 20 mrads to 35 mrads [5]. The angle subtended by the source is called the local divergence angle θ_s.

2.1 Plane Wave Representation & Propagation Method

The incident electric field for a wavelength λ can be written as

$$E^{in}(x, y, z; \lambda) = Ee^{i[(k_x\hat{x}+k_y\hat{y}+k_z\hat{z})+\phi(x,y,z)]} \tag{1}$$

where $k_x^2 + k_y^2 + k_z^2 = k^2 = (\frac{2\pi}{\lambda})^2$.

The propagation of the incident field through the mask is done using a layering scheme [6]. In this the mask-gap-resist system is treated a stack of thin layers; the image is propagated one layer at a time. The incident field for $(i + 1)$th layer is the output field of ith layer. In each layer the propagation is done using the *angular spectrum propagation method* [7]. Once the absorbed dose in the resist is computed, it is converted to a dissolution rate appropriate to the resist. A development model based on a "level set" approach [8], is used to obtain the final developed pattern.

2.2 Angular Blur

The concept of *angular blur* is illustrated in Figure 3. The electric field at each point (x, y) in a resist layer has contributions from several points on the mask due to the finite size of the source. For example, the electric field in the shaded region contributes to the point at the tip of the cone in the resist. These contributions can be either *coherent*, *partially coherent* or *incoherent*. For our purpose, the case of complete incoherence is important as it is a reasonable assumption for laser driven plasma sources. However, we first give the expressions for coherent case.

2.2.1 Coherent Case

This case is mathematically simple, as we have to just add the electric field contributions from the mask at each point in the resist. This can be shown to be equivalent to filtering in the Fourier domain. The expressions are given below.

Let the exiting electric field at the mask be denoted by $E_m(x, y)$. Let

$$F_m(f_x, f_y) = \int_{-\infty}^{\infty}\int E_m(x, y)e^{-j2\pi(f_x x+f_y y)}dxdy \tag{2}$$

denote the two-dimensional Fourier transform of $E_m(x, y)$. We can now write $E_m(x, y)$ as a superposition integral.

$$E_m(x, y) = \int_{-\infty}^{\infty}\int F_m(f_x, f_y)e^{j2\pi(f_x x+f_y y)}df_x df_y \tag{3}$$

Now the field in a resist layer can be written as,

$$E_r(x, y) = \int_{-\infty}^{\infty}\int F_m(f_x, f_y)e^{j2\pi(f_x x+f_y y)}P(f_x, f_y, D)B(f_x, f_y, D, \theta_g, \theta_s)df_x df_y \tag{4}$$

where

$$P(f_x, f_y, D) = e^{j\frac{2\pi}{\lambda}D\sqrt{1-(\lambda f_x)^2-(\lambda f_y)^2}} \tag{5}$$

is the free space propagation kernel and

$$B(f_x, f_y, D) = \begin{cases} \frac{1}{A} & (\frac{f_x}{2(1-cos(\frac{\theta_s}{2}))})^2 + (\frac{f_y}{2(1-cos(\frac{\theta_s}{2}))})^2 \leq 1 \\ 0 & otherwise \end{cases} \tag{6}$$

is the angular blur filter and A is the area of the ellipse. The above expression can be easily obtained with some geometrical calculations over the cone. With a little bit more algebra, it can be shown that

$$A = \pi D^2(tan(\theta_g + \theta_s) - tan(\theta_g + \frac{\theta_s}{2}))^2 \tag{7}$$

for a circular source. We can generalize this for an elliptical source as,

$$A = \pi D(tan(\theta_{gx} + \theta_{sx}) - tan(\theta_{gx} + \frac{\theta_{sx}}{2}))D(tan(\theta_{gy} + \theta_{sy}) - tan(\theta_{gy} + \frac{\theta_{sy}}{2})) \tag{8}$$

From the above expressions, it is clear that the *angular blur* acts as a moving average filter. The dependence on the value D shows that the blur increases as we go down to the bottom layers of the resist.

2.2.2 Case of Incoherence

If the source subtended angle $\theta_s = \frac{\Delta s}{D}$ is smaller than the diffraction angle λf - where Δs is the geometrical shadow on the resist - then we can fall back on a simplified convolution approach shown below. The intensity at a point (x, y) in a resist layer can be expressed as an integration over the source region.

$$I_r(x, y) = \int_{a_s} I_r(x, y; x_s, y_s) dx_s dy_s \tag{9}$$

where the integration is performed over the source area a_s. Assuming a spatial invariance, this can be written as a convolution integral,

$$I_r(x, y) = \int_A I_r(x', y') B(x - x', y - y') dx' dy' \tag{10}$$

with $B(x, y)$ being the blur function.

If $\theta_s \approx \lambda f$ then the source must be sampled and the intensity contributions should be added. This effect is related to the failure of the Kirchhoff approximation for thick absorbers (Sommerfeld line edge field)[9] and decays as $\frac{1}{r^2}$ where r in this case is gap. For "usual" cases $D \approx 10 - 20\mu$m the convolution is a sound approximation. In the case of incoherent source the finite extent of the source gives once more origin to a low pass filter. The case of partial coherence is more complicated and not discussed here. In this paper we assumed the incoherent case for our simulations.

Table 1: Simulation Parameters

θ_g	CD	$\theta_{sx} = \theta_{sy}$	mask-to-wafer gap	Absorber	Resist
20mrads	100nm	1.7mrads	15μm	Au(450nm)	APEX-E(500nm)

3 Computational Results

For the modeling study, we first considered an isolated-lines and then a complex mask pattern. The values used for various parameters are listed in the table below.

The profiles of the absorbed dose are shown in Figure 4. Notice the shift from the top to the bottom of the resist. The approximate shift was found to be 20nm. In order to compare, we considered a collimated beam from a point source. The divergence angle for a typical collimated beam is about 5mrads [6]. Figure 5 shows the absorbed dose profiles from top to bottom of resist. The lateral shift is quite less in this case.

Figures 6 and 7 show the cross section of developed profiles for the uncollimated and collimated cases. It can be seen that a divergence angle of 5mrads has barely any effect on the sidewall slope whereas a divergence angle of 20mrads results in a significant difference in the sidewall slopes.

3.1 A complex pattern

Figure 12 shows a complex mask pattern, where each feature has a line width of 130nm. The simulation parameters are the same as that of the previous case, except that the mask-to-wafer gap is 10μm. The cross-section of the aerial image is also shown. The developed pattern is shown in Figure 13. Notice the wedged developed features in addition to the lateral shift caused by the divergence angles. There is also significant loss in resist thickness.

4 Conclusions

In this article, we presented an extension the modeling of image formation to point sources. We modeled the finite size of the source as an angular blur. Computationally, this is equivalent to a moving average filter on the electric field in each layer. The global divergence angle θ_g causes a lateral shift in the aerial image. The source divergence angle causes a reduction in contrast of the aerial image, while filtering high frequency components. The angular blur increases linearly with mask-to-wafer gap. For large gaps, this may result in the complete dissolution of the resist with no features left.

References

[1] Cerrina F., *X-ray Lithography*, Chapter 3, Handbook of Microlithography, Micromachining and MicroFabrication, Volume 1, 1997.

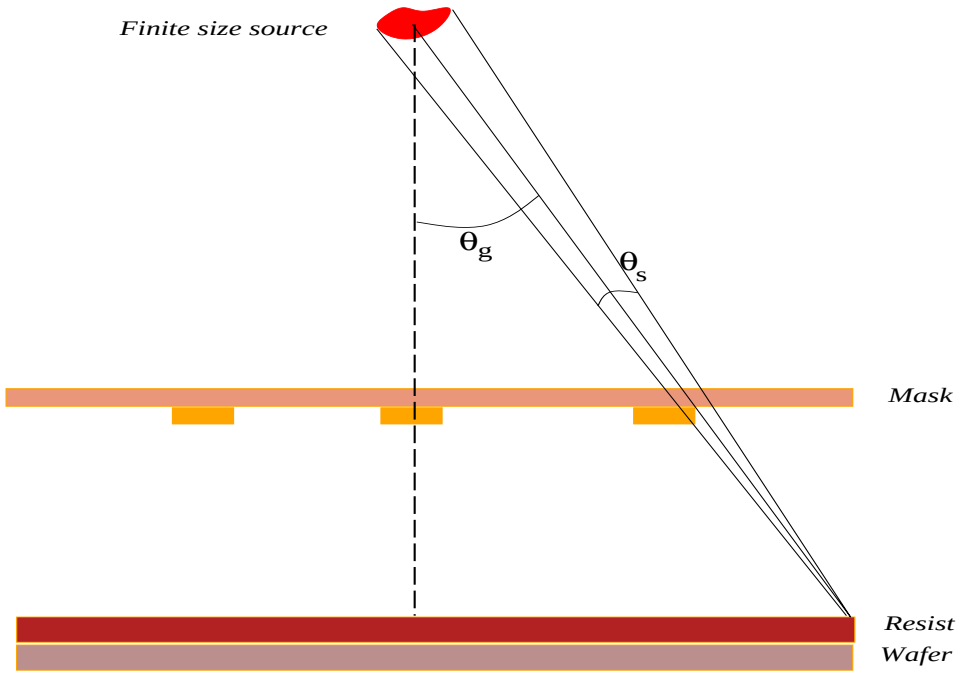

Figure 1: *Illustration of divergence angles due to a point source. θ_g is the global divergence angle and θ_s is the local divergence angle.*

[2] Prasad R. R., Krishnan M., Mangano J., Greene P. A., Qi N., *Neon dense plasma focus point x-ray source for sub-0.25μm lithography*, SPIE Proc., **2194**, 120(1994).

[3] Plidden S.C., Richter M. R., Hammer D. A., Kalantar D. H., *1-kW x-pinch soft x-ray source*, SPIE Proc., **2194**, 209(1994).

[4] R. Fedosejevs, R. Bobkowski, J. N. Broughton and B. Harwood, *keV X-ray source based on high repetition rate excimer laser-produced plasmas*, SPIE Proc., Vol **1671**, pp 373-382, 1992.

[5] M. Vartanian and D. Gibson, *Development of polycapillary collimator for point source x-ray lithography*, SPIE Proc., Vol **1924**, pp 335-342, 1993.

[6] Bollepalli B. S., Khan M., Cerrina F., *Image formation in X-ray lithography: A layer based approach*, TECHCON, 1996.

[7] Joseph W. Goodman, *Introduction to Fourier Optics*, McGraw-Hill Book Company, 1968.

[8] Sethian J., *A Fast Marching Level Set Method for Monotonically Advancing Fronts*,Center for Pure & Applied Mathematics, UC Berkeley, Report PAM-652.

[9] Guo Jerry, Cerrina F., IBM Journal of Res. & Dev., July 1993.

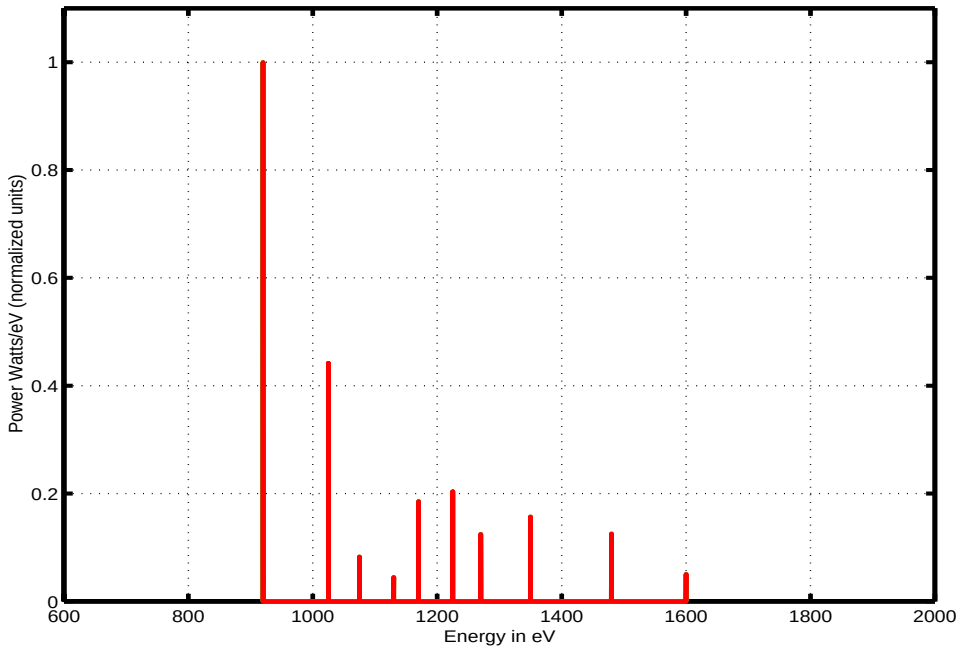

Figure 2: *A typical spectrum due to a point source*

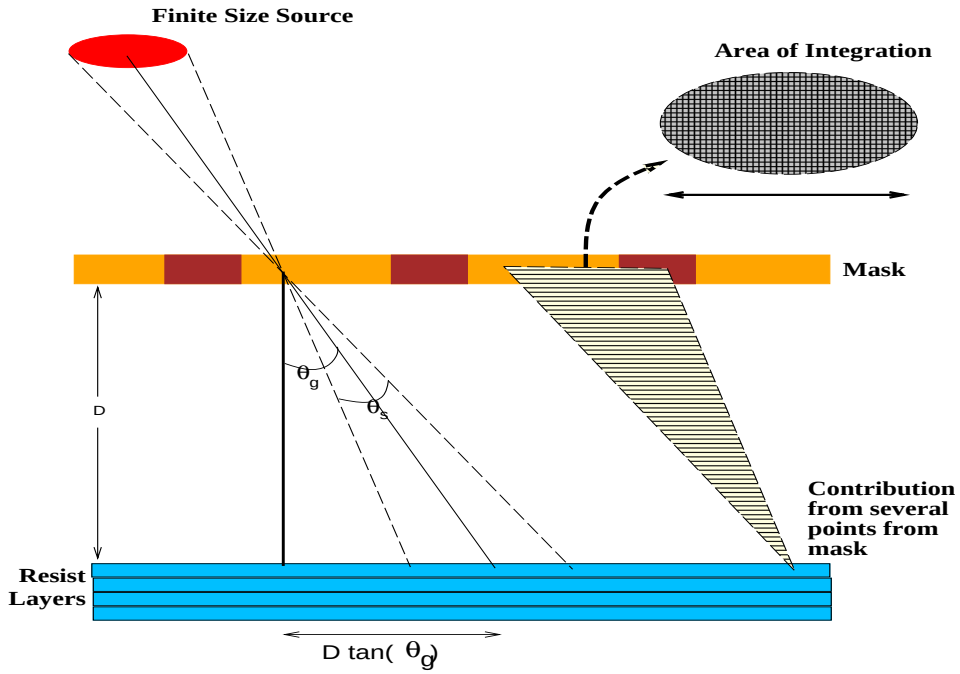

Figure 3: *Illustration of angular blur concept*

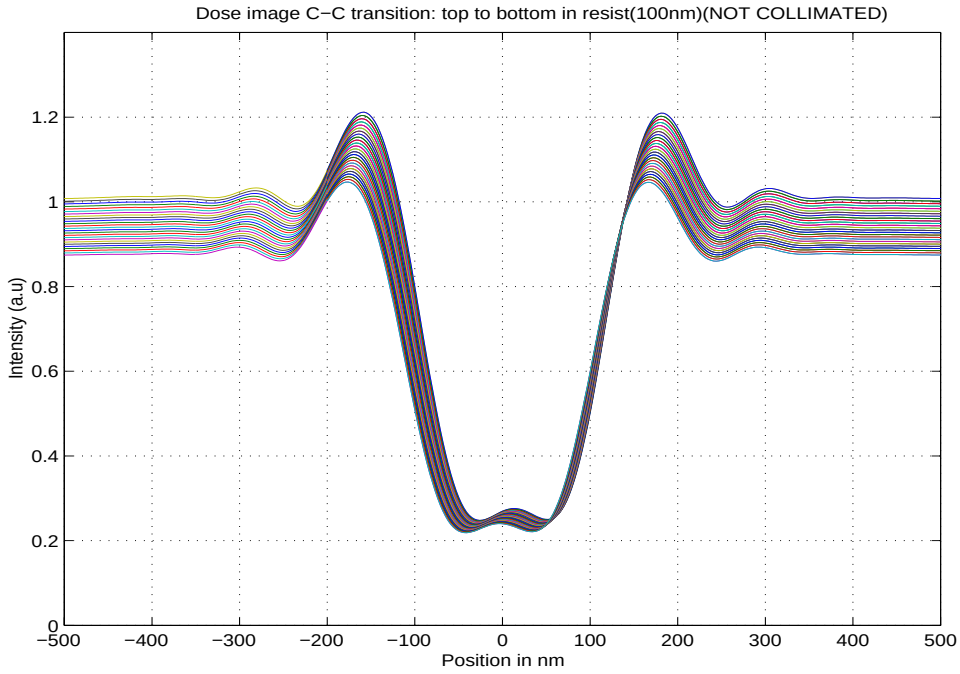

Figure 4: *Cross-section of absorbed dose in the resist layers from top to bottom. Notice the sideways shift due to the divergence angle* θ_g.

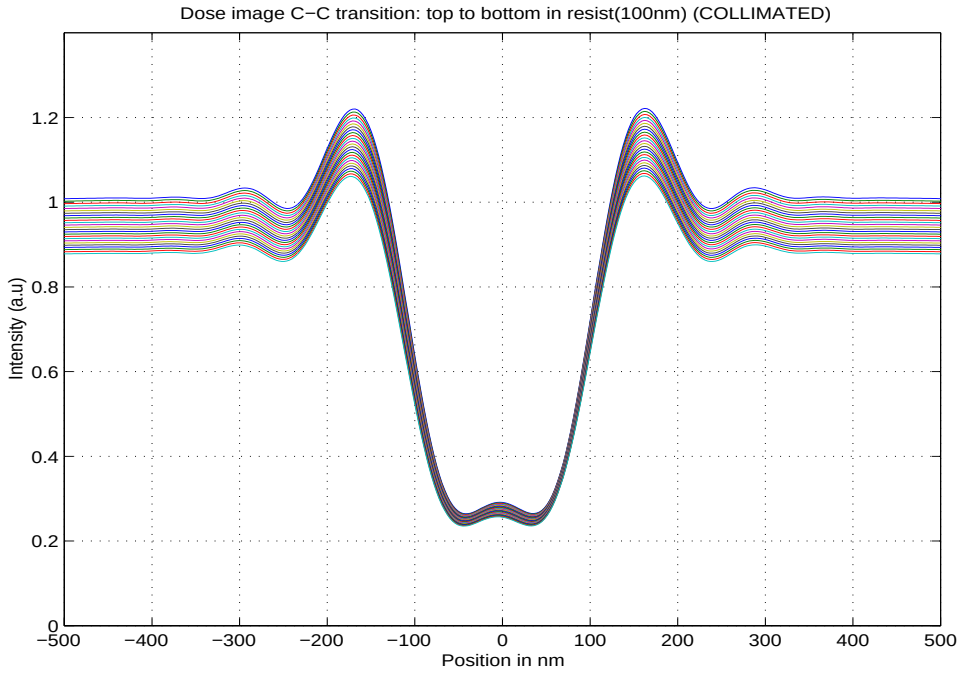

Figure 5: *Cross-section of absorbed dose in the resist layers from top to bottom. The sideways shift is less because of a collimated beam with low divergence angle.*

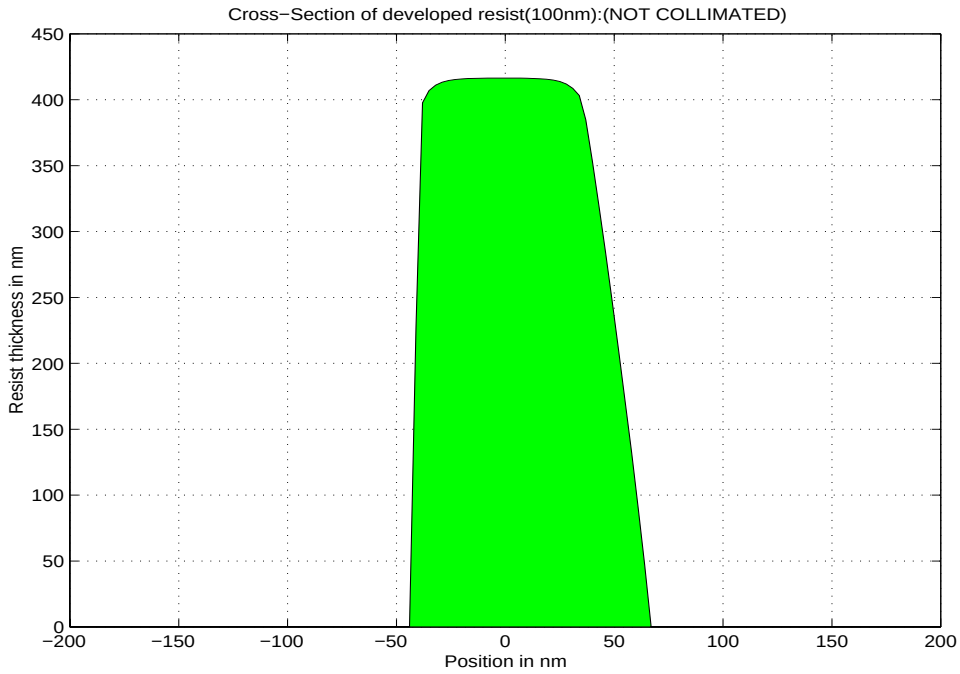

Figure 6: *Cross-section of the developed profile of an isolated-line pattern. The asymmetrical side-wall slopes are due to* θ_g.

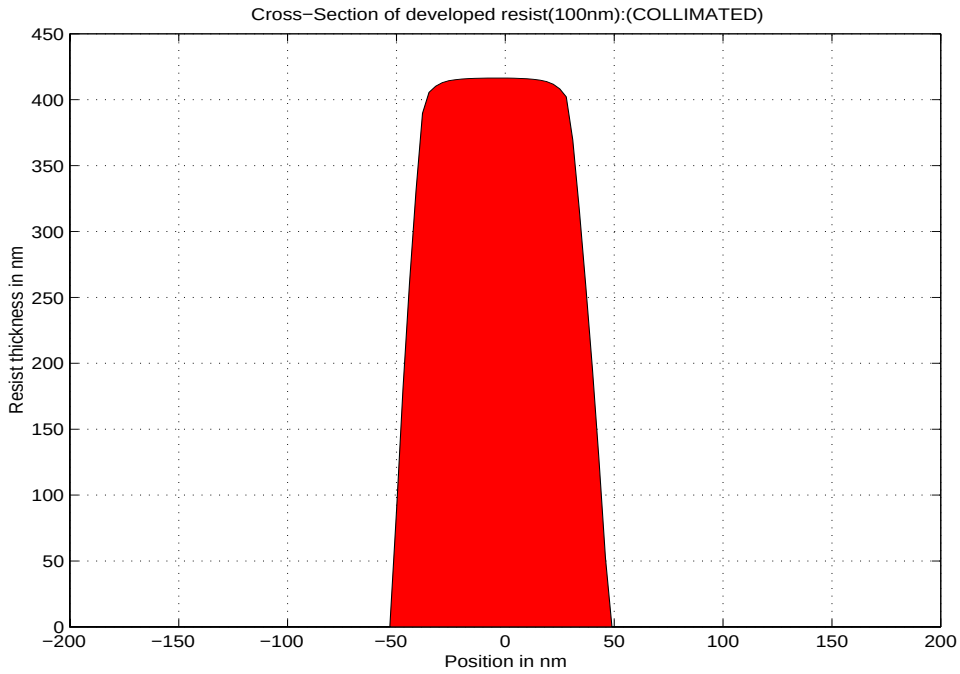

Figure 7: *Cross-section of the developed profile of an isolated-line pattern due to a collimated incident beam.*

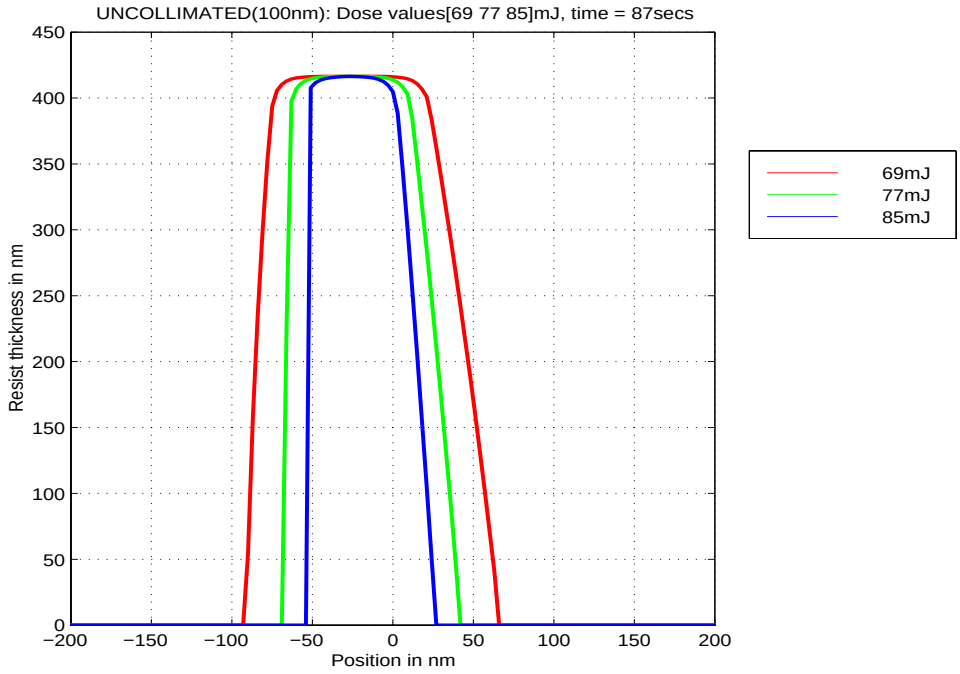

Figure 8: *Illustration of dose latitude. The three profiles correspond to a nominal dose, +10% and -10% values for APEX-E resist. The large variation is due to divergence angle.*

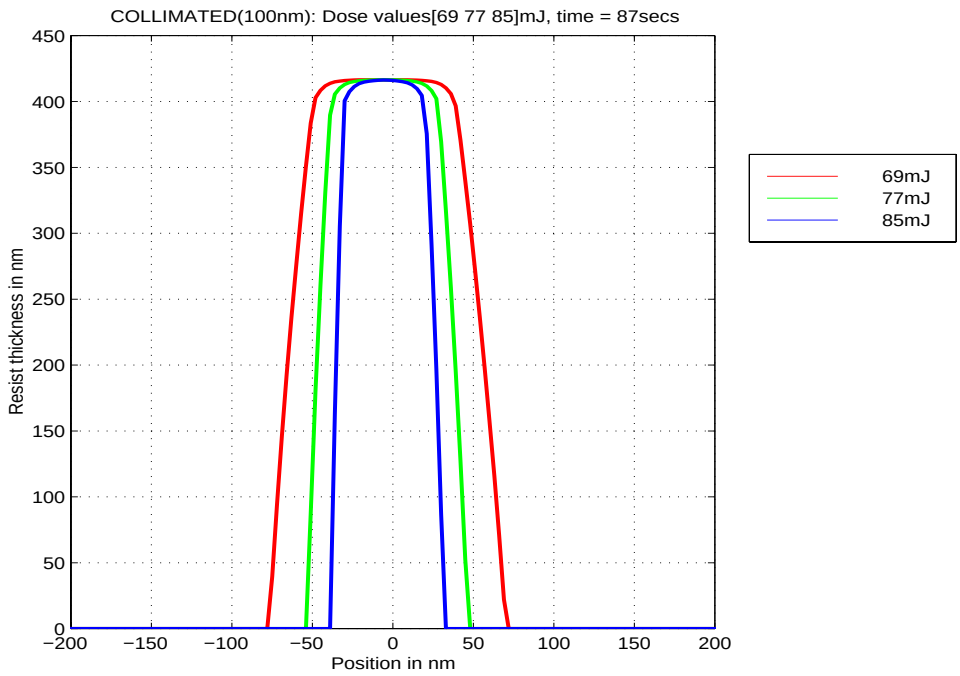

Figure 9: *Illustration of dose latitude. he three profiles correspond to a nominal dose, +10% and -10% values for APEX-E resist. This is the case for collimated incident beam.*

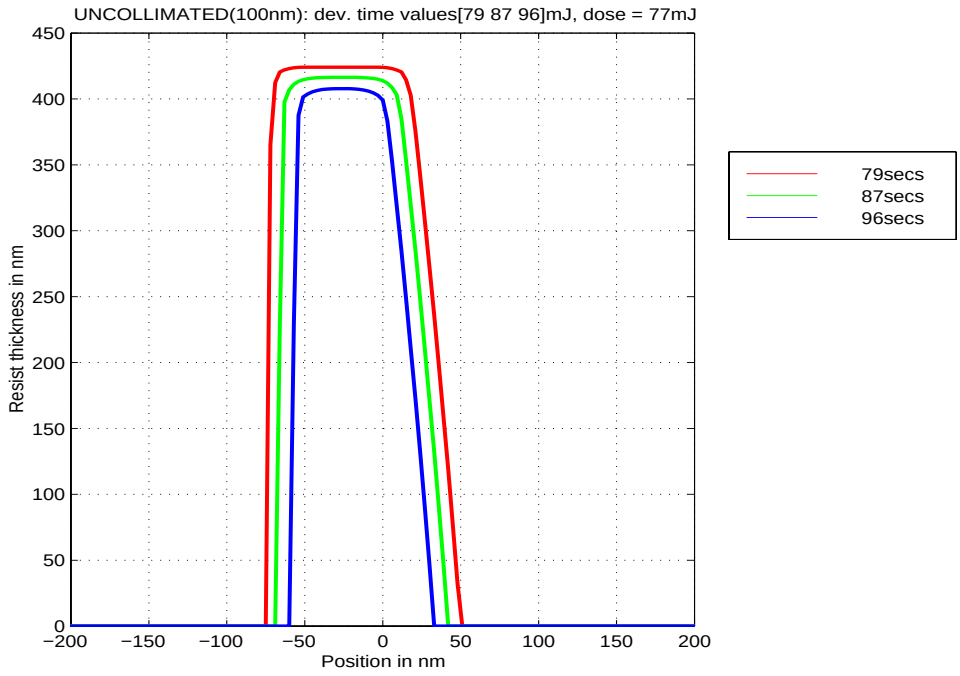

Figure 10: *Illustration of development time latitude. The three profiles correspond to a nominal development time, +10% and -10% values for APEX-E resist.*

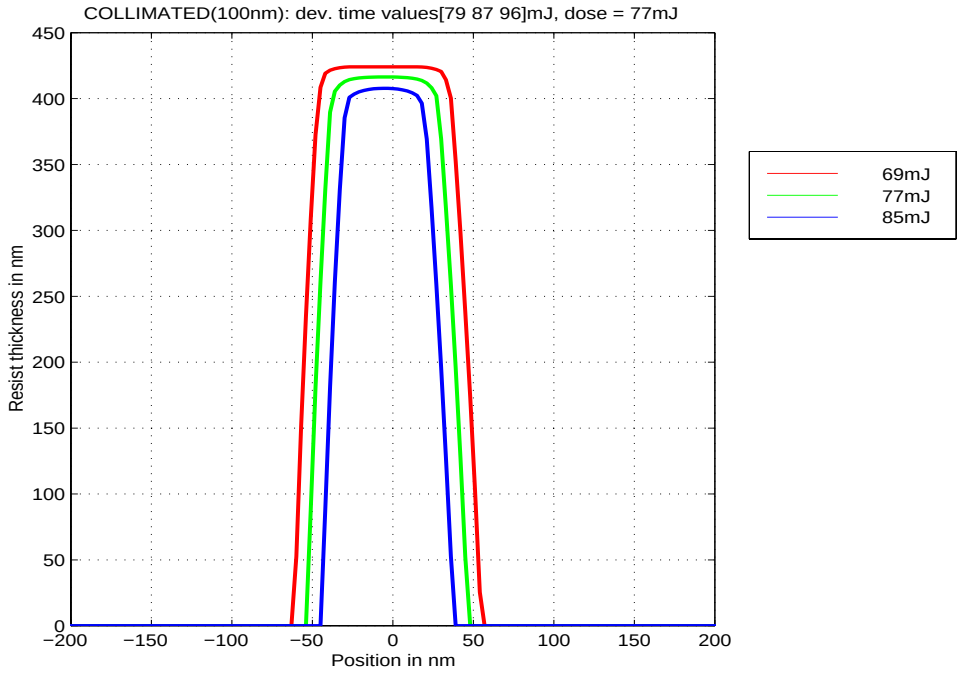

Figure 11: *Illustration of time latitude for the collimated case.*

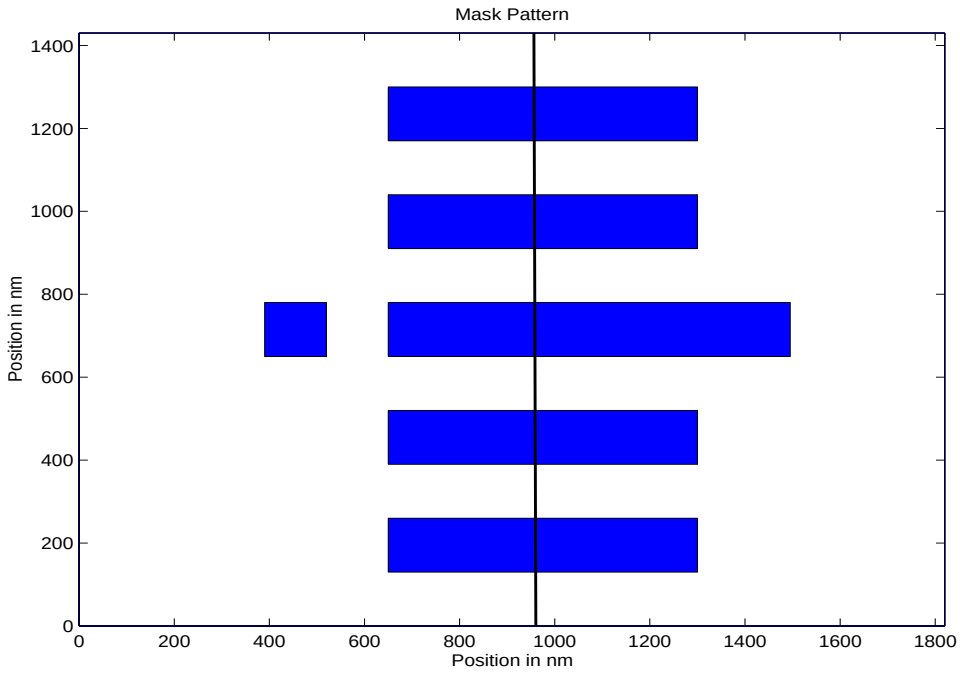

Figure 12: *A complex pattern. The aerial image cross-sections are shown in figure 13.*

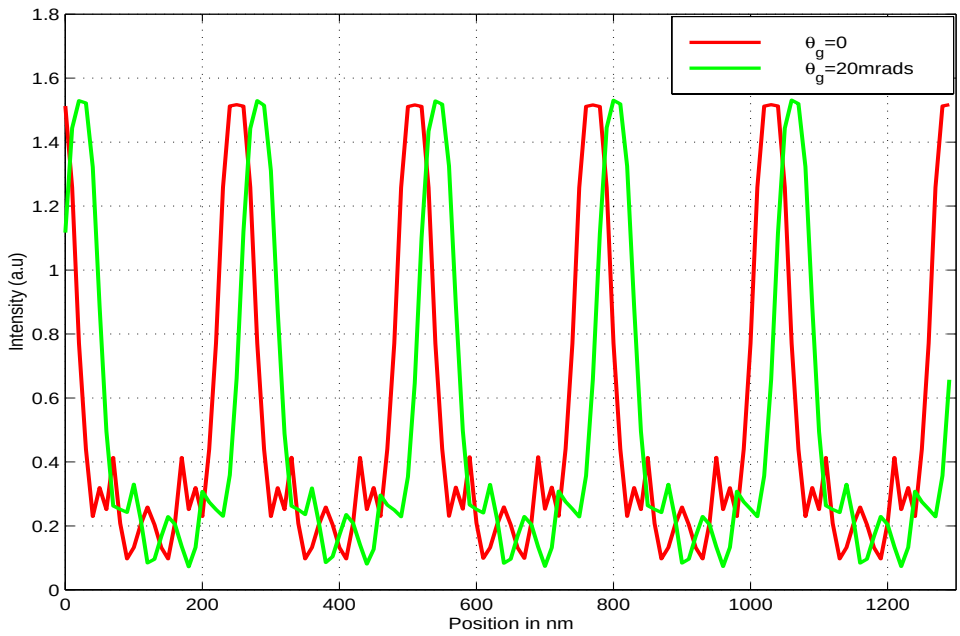

Figure 13: *Cross-section of aerial images due to normal incidence and oblique incidence (the mask is shown in figure 12). Notice the shift.*

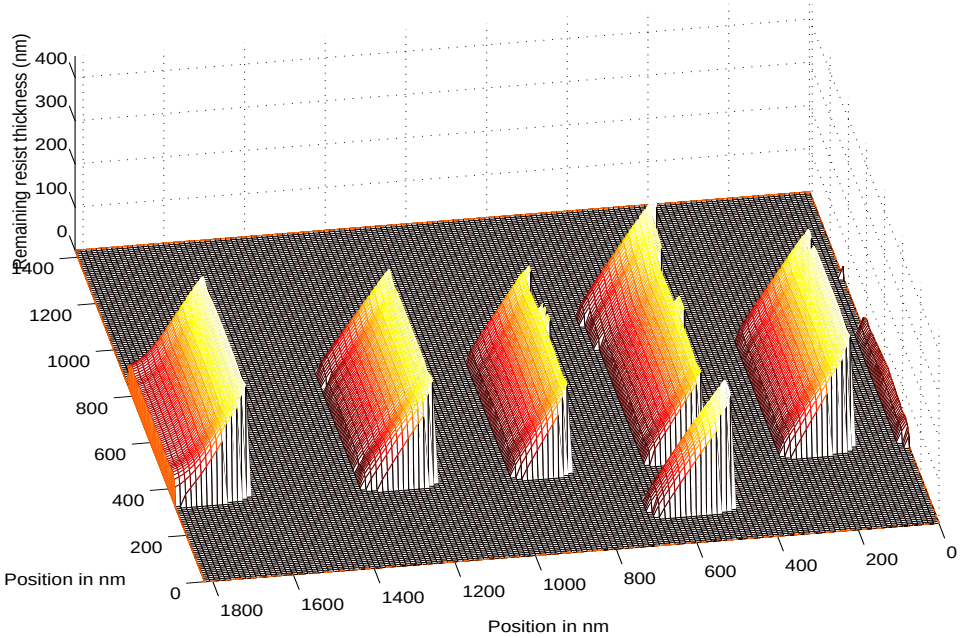

Figure 14: *Developed resist profile for the complex pattern*